

†Supporting Information

Impact of Bi and its oxide phases on Bi₂S₃ compound transformation and photoelectrochemical performance

Erhon Leonetti Aragão,^a Ariadne Köche,^a Gabriela Corati Touguinha,^b Johnny Ferraz Dias,^b Larissa dos Santos Stein,^a Julia Machado Barradas,^a Anderson Thesing^a, and Sherdil Khan^{*a}

^a Laboratory of Nanomaterials for Renewable Energy and Artificial Photosynthesis (NanoREAP), Institute of Physics, Federal University of Rio Grande do Sul (UFRGS), Campus do Vale, Agronomia, Porto Alegre-RS, Brazil.

^b Ion Implantation Laboratory, Institute of Physics, Federal University of Rio Grande do Sul (UFRGS), Campus do Vale, Agronomia, Porto Alegre-RS, Brazil.

[*sherdil.khan@ufrgs.br](mailto:sherdil.khan@ufrgs.br)

Section S1 – Experimental procedure

Sputtering deposition of metallic Bi onto FTO substrate

Prior to deposition, fluorine-doped tin oxide (FTO)-coated glass substrates 2 cm × 1 cm (Sigma Aldrich, resistivity ~7Ω/sq) were cleaned ultrasonically with deionized water and detergent followed by acetone, for 20 min each. Metallic Bi was deposited using an RF magnetron sputtering equipment (Orion-8, AJA) at 2 mTorr Ar pressure, with deposition times of 10, 40, and 100 min. Based on the deposition rate calculated for the Bi target (0.84 Å s⁻¹), samples yielded deposited layers of approximately 50, 200, and 500 nm for deposition times of 10, 40, and 100 min, respectively. The RF power applied to the Bi target was kept at 25 W for all depositions.

Thermal oxidation and sulfurization

The obtained metallic Bi thin films underwent thermal oxidation at 250 °C and 550 °C in ambient air to produce bismuth oxide (Bi₂O₃) films. The heating rate used was 5 °C min⁻¹ and samples were calcinated for 1 h (for temperature 550 °C) and 5 h (for the 250 °C one). For sulfurization, 2.5 g of sulfur (S) (Dinâmica, 99.5%) was placed in a crucible located at the end

of a quartz tube and Ar 99.999% (50 mL/min) was used as carrier gas. The prepared films were placed downstream at 15 cm from the S crucible in a tube furnace heated at 300 °C for 3 h, with a heating rate of 10 °C min⁻¹. Finally, the films were naturally cooled down to room temperature under Ar flow. Figure S1 illustrates the experimental procedure for the synthesis process and sulfurization in the tube furnace. Additionally, for comparison, we also produced Bi₂O₃ at 550°C for 5 h in air, followed by sulfurization. The XRD and LSV data obtained for this sample is presented in Figures S9 and S16, respectively.

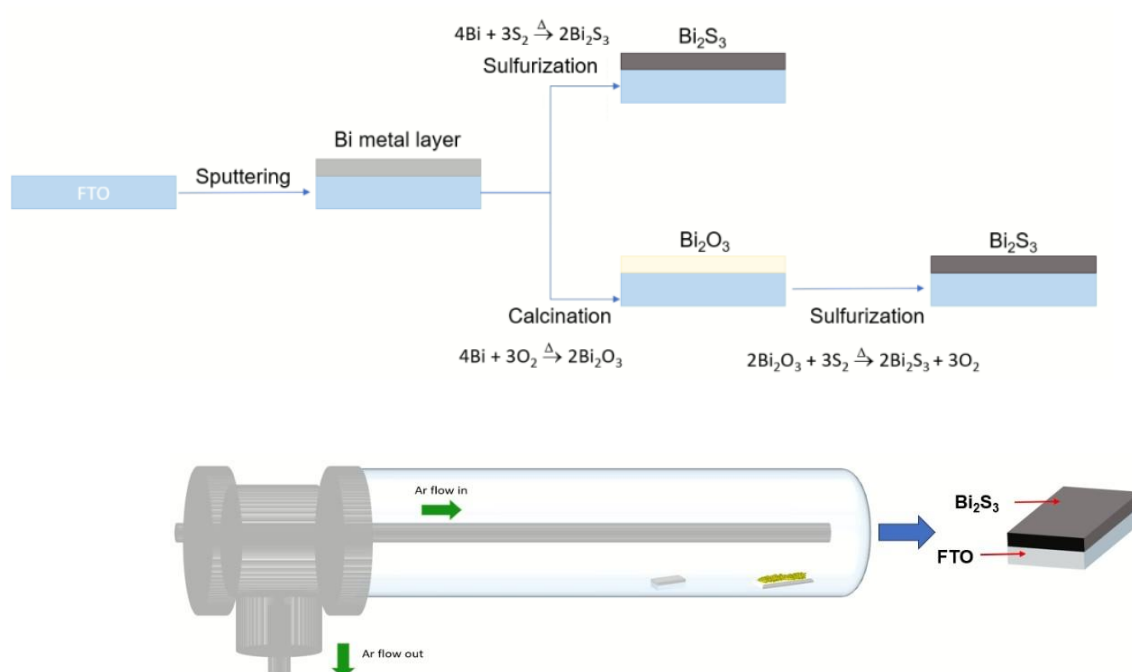


Figure S1. (Top) Schematic of the synthesis procedure for Bi films deposited by magnetron sputtering, including as-deposited and oxidized films prior to sulfurization. (Bottom) Sulfurization setup featuring a closed-end quartz tube with the sample films positioned 15 cm from the sulfur powder, using Ar as the carrier gas heated in a tube furnace at 300 °C for 3h.

Characterization

The morphological properties of thin films were evaluated by scanning electron microscopy (SEM, JSM-6610LV, JEOL and Zeiss SEM-FEG/GIB Auriga) with an acceleration voltage of 20 kV. The crystalline structure of the films was analyzed by GIXRD (Bruker D8 Advance) with a grazing angle of 5° using Cu $K\alpha$ radiation with 2θ ranging from 15 to 80° with a 0.02° step size and measurement time of 3 s per step. Obtained XRD data was indexed using the International Centre for Diffraction Data (ICDD) - PDF2 database. The average crystallite size was obtained by employing the Debye-Scherrer equation,^[34] considering $k = 0.94$. X-ray Photoelectron Spectroscopy (XPS) technique was obtained with an OMICRON (CHA - Concentric Hemispherical Analyser) equipment, using Al/ $K\alpha$ (1486.6 eV) radiation, anode operated at 15 kV, 15 mA and 225W, and filament operated at 4 A. The survey spectrum was obtained with 50 eV and step of 1 eV and high-resolution data was recorded with 10 eV and step of 0.1 eV. The software used to analyze XPS data was CasaXPS with calibration based on the adventitious carbon peak using 285 eV. The absorption spectra of the thin films on FTO were measured using a spectrophotometer (Varian Cary 5000) in the ultraviolet-visible (UV-vis) range. Assessments of the PEC performance of the obtained thin films were performed using linear sweep voltammetry curves (LSV) employing a three-electrode configuration using a Pt counter electrode and Ag/AgCl (saturated KCl) reference electrode under a 0.1 M Na_2S electrolyte. The measurements were made using a scan rate of 20 mV s^{-1} from open circuit potential to 0 V versus reversible hydrogen electrode (RHE) using a potentiostat (ZRA Interface 1000 Gamry). The area of the photoelectrode was defined to 1 cm^2 and PEC tests were performed under a Xenon lamp at 100 mW cm^{-2} using an AM 1.5 G filter (ScienceTech). All potentials have been converted to the RHE scale according to the following equation, where $E_{\text{Ag/AgCl}}$ is the potential relative to the Ag/AgCl electrode.

$$E_{\text{RHE}} = E_{\text{Ag/AgCl}} + 0.197 + 0.0591 \times \text{pH}$$

Long-term stability tests were conducted using chronoamperometry at a constant potential of 1.23 V vs RHE. Each measurement consisted of three phases: an initial 30 s dark period to establish baseline current, followed by 30 min of continuous illumination (100 mW cm⁻²), and a final 30 s dark period to monitor current decay.

Additionally, we performed stability tests, quantifying the relative photocurrent loss during operation by analyzing the difference between the photocurrent upon illumination (J_{on}) and after light is turned off (J_{off}). The percentage of photocurrent loss was calculated using the following expression:

$$\text{Photocurrent Loss (\%)} = \left(\frac{J_{off}}{J_{on}} \right) \times 100$$

Open-circuit potential (OCP) measurements were performed under intermittent illumination to evaluate photoresponse characteristics. The OCP gain was determined from the potential difference between illuminated and dark conditions at steady state. Charge carrier recombination dynamics were analyzed by monitoring the OCP decay with an exponential function following light extinction. Electrochemical impedance spectroscopy (EIS) was performed at open-circuit potential under illumination, with an amplitude of 10 mV using V vs E_{OC} over a frequency range of 100 kHz to 100m Hz.

X-ray fluorescence (XRF) mapping

An X-ray fluorescence (XRF) mapping experiment was performed at the Carnáuba beamline (Tarumã station) of the Brazilian Synchrotron Light Laboratory (LNLS), located at the National Center for Research in Energy and Materials (CNPEM). The XRF mapping was carried out in continuous scan mode at room temperature using a nano probe with dimensions of 200 x 500 nm² over a 200 x 200 μm^2 sample area. The excitation energy was set to 13440.0 eV with a constant ring current at 200.0 mA.

Rutherford Backscattering Spectrometry (RBS) analysis

Samples were analyzed with the Rutherford Backscattering Spectrometry (RBS) technique in order to study the film thickness and understand the process of sulfur diffusion into the films. Thus, the elemental profile of the samples was determined. In this study, a 3 MeV He⁺ beam with typical currents of about 10 nA was employed. Backscattered particles were detected with a silicon surface barrier detector with an energy resolution of about 20 keV and placed at 165° with respect to the beam direction. The obtained spectra were analyzed through a simulation process using the PowerMEIS3 software (available at tars.if.ufrgs.br).¹ The simulation process considers important physical parameters and sample information, including its composition, stoichiometry and the elemental depth profile. Usually, the analysis of RBS data is based on the simulation of the spectrum where several parameters of the experimental setup and of the sample under analysis can be adjusted in order to provide the best fit for the spectrum. The sample description may consist of different layers with varying compositions and elemental concentrations. However, the interface between different components usually exhibits a complex structure, making the fitting process more challenging. This complexity is mainly due to the diffusion of elements between layers which, in the present case, was identified by the low energy edge signal in the spectrum at Bi, Sn (from SnO₂ in FTO) and S regions, indicating the presence of concentration gradients. Basically, to analyze the diffusion, additional layers with intermediate compositions are added to simulate the mixture at the interface. Through this method, it is possible to deduce (approximately) the fraction of each element in the mixture and its thickness. During the simulation process, the addition of intermediate layers of Bi, Sn, S and compounds of different structures allows for a detailed description of the experimental spectra. During analysis of both sulfurized oxide-based

¹ M. A. Sortica and others, 'Characterization of Nanoparticles through Medium-Energy Ion Scattering', *Journal of Applied Physics*, 106.11 (2009), p. 114320, doi:10.1063/1.3266139;

G.G.Marmitt, 'PowerMEIS-3 Simulation Code' <<http://tars.if.ufrgs.br/>>.

and the pristine (standard) Bi_2S_3 films, 3–4 intermediate layers were included to improve fitting, corresponding to diffusion regions at the film/substrate (FTO) interface. Layers were classified as principal (Bi_2O_3 or Bi_2S_3) or intermediate, based on elemental concentration dominance over SnO_2 . Thickness evaluation followed this criterion. Data are shown in Table S1, detailing both pure films and intermediate regions with FTO diffusion.

Section S2 – Results and Discussion

To optimize the obtained films employed in this work, we tested different deposition times for metallic Bi films. Based on the deposition rate mentioned above (Section S1), the films thickness was estimated at 50, 200 and 500 nm for deposition times of 10, 40, and 100 minutes, respectively.

Based on the X-ray diffraction (XRD) patterns of obtained films after sputtering deposition and prior to any calcination (Figure S2), we observed more intense peaks related to metallic Bi (JCPDS #85-1331) with longer deposition times. Moreover, the surface of all deposited thin films was homogeneous, based on SEM analysis (Figure S4), with no significant difference among varied deposition times.

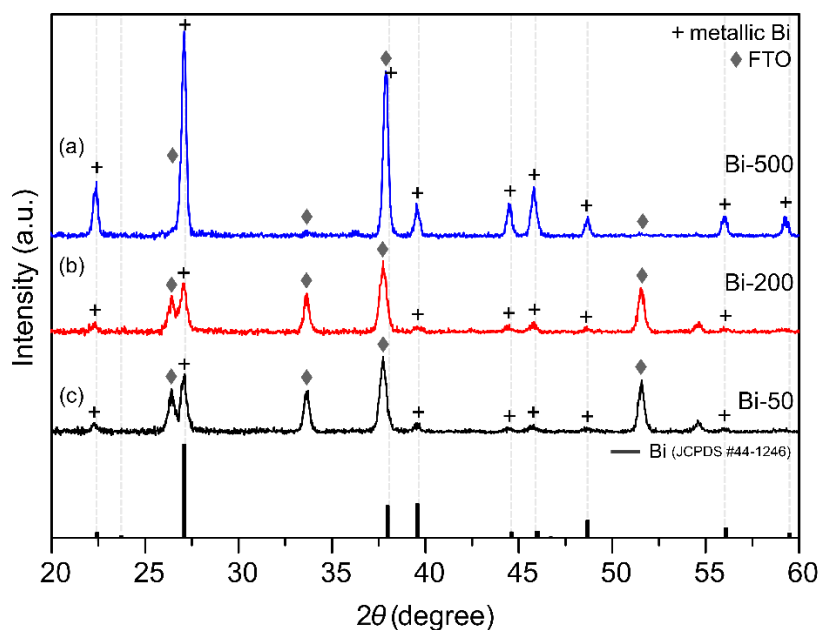


Figure S2. XRD patterns of the Bi films deposited via RF magnetron sputtering with deposition times of 10, 40, and 100 min, keeping the target RF power constant.

As-deposited samples that underwent direct sulfurization were analyzed by XRD (Figure S3). All obtained sulfurized samples exhibit diffraction patterns associated with an orthorhombic Bi_2S_3 phase (JCPDS #65-2431), along with peaks related to the FTO substrate. The crystallite size was calculated as 19.3, 20.0, and 21.4 nm, for samples with 10-, 40-, and 100-min deposition time, respectively, showing a slight increase in crystallinity for thicker films.

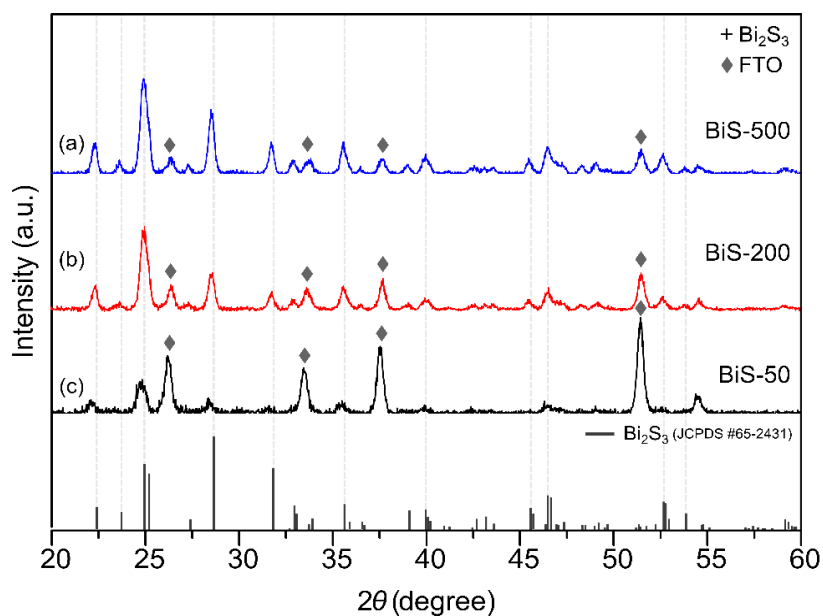


Figure S3. XRD patterns of the sulfurized Bi films deposited with deposition times of (a) 100, (b) 40, and (c) 10 min, keeping the target RF power constant. The FTO peaks decrease with the deposition time due to an increase in the film thickness.

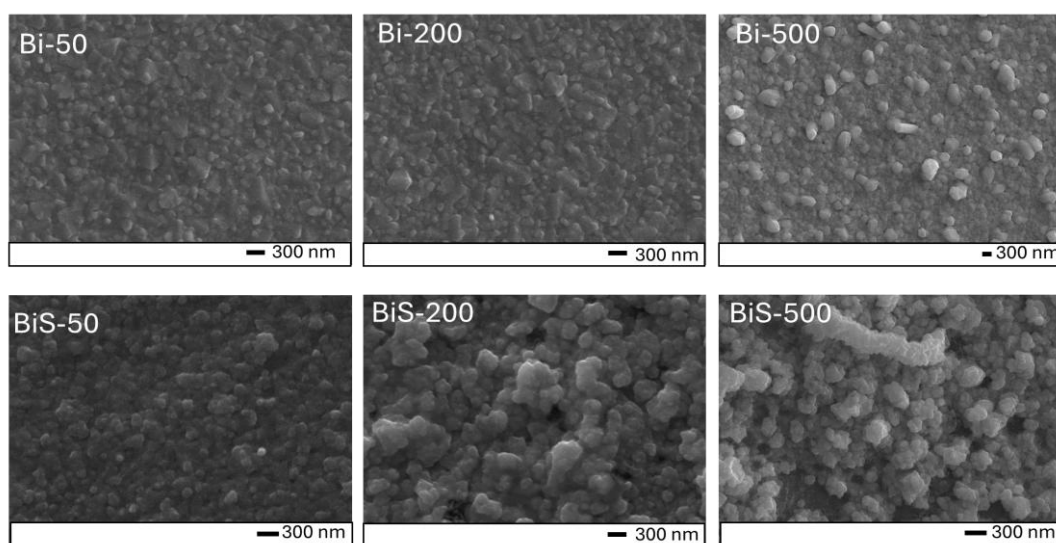


Figure S4. SEM images of as-deposited metallic Bi thin films prepared at deposition times of 20, 40, and 100 minutes (top row), alongside their corresponding sulfurized Bi_2S_3 films (bottom row).

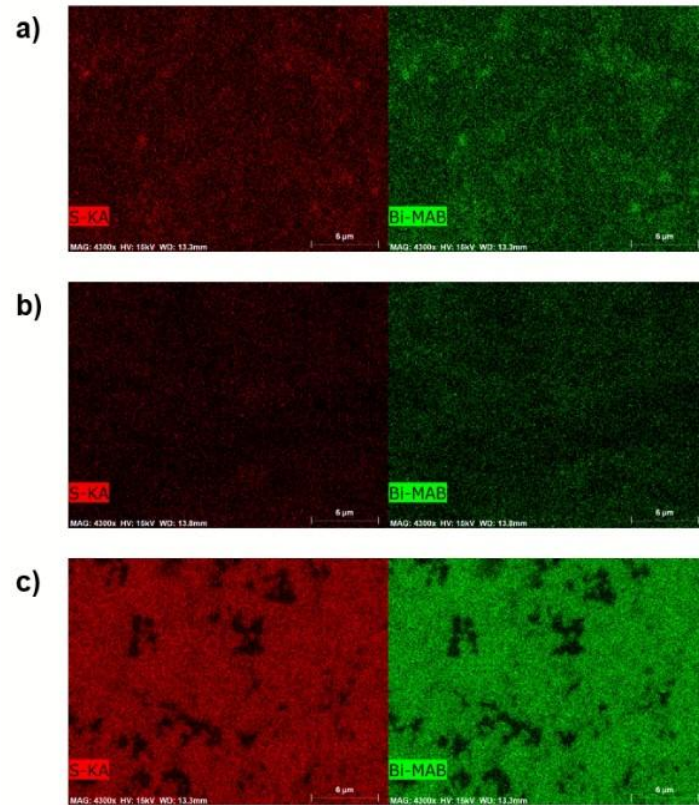


Figure S5. EDS mapping of sulfurized Bi_2S_3 films, showing that Bi and S are uniformly distributed over the film surface (a) BiS-50, (b) BiS-200 and (c) BiS-500.

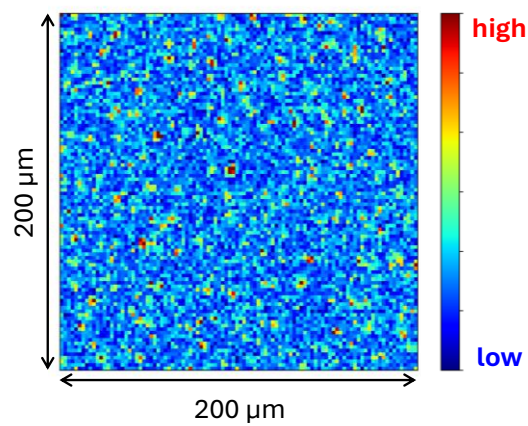


Figure S6. XRF mapping of Bi for BiS-200 sample after sulfurization.

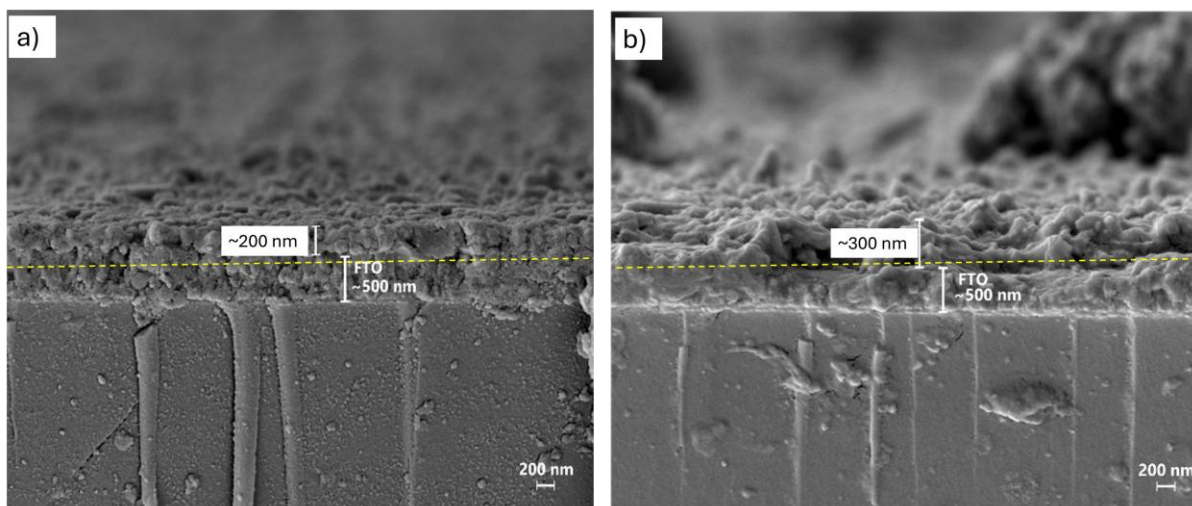


Figure S7. Cross section SEM images of as-deposited Bi film (a) Bi-200 and its corresponding sulfurized Bi_2S_3 film (b) BiS-200. The film thickness increases after the sulfurization process due to the incorporation of S into Bi matrix.

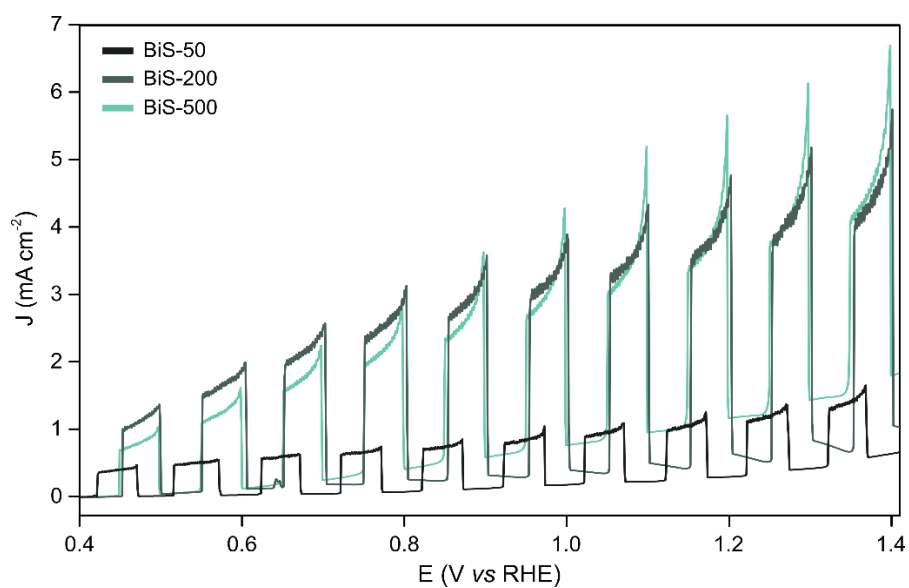


Figure S8. Chopped LSV curves of the sulfurized Bi films deposited with deposition times of 10, 40, and 100 min, named as BiS-50, BiS-200 and BiS-500, respectively.

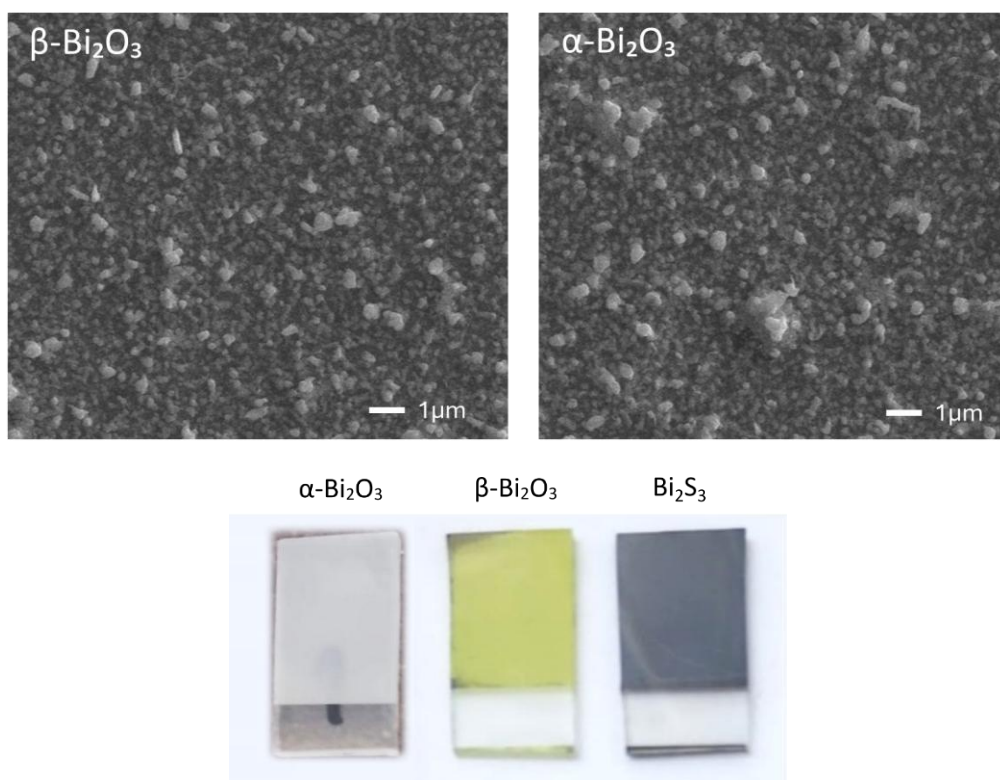


Figure S9. (Top images) SEM images of Bi-200 films oxidized at 250 °C for 1h in air to produce (a) β - Bi_2O_3 and 550 °C for 5h to produce (b) α - Bi_2O_3 . (Bottom Image) Visual comparison of samples submitted to thermal oxidation and sulfurization process (both oxides produced sulfurized films with similar coloration), as described in the image.

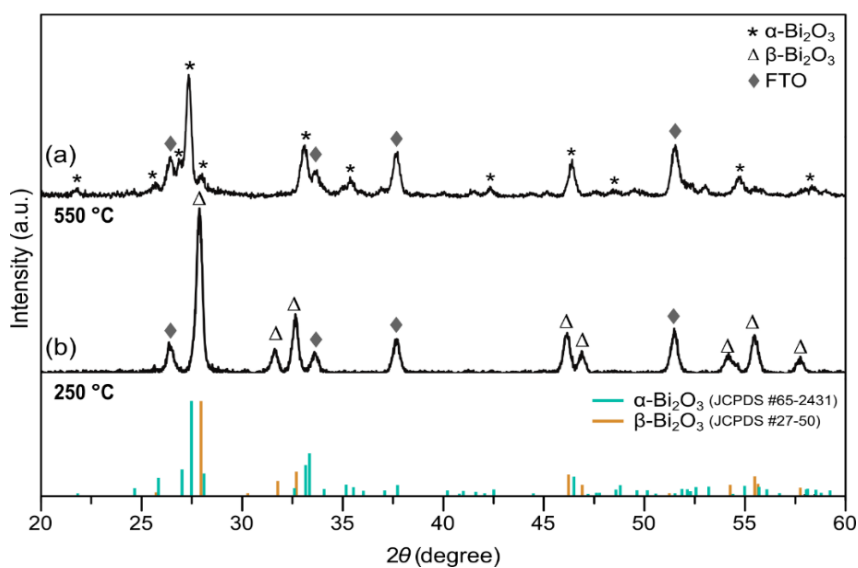


Figure S10. XRD patterns of thermally oxidized samples prior to sulfurization, depicting the two different Bi_2O_3 obtained phases.

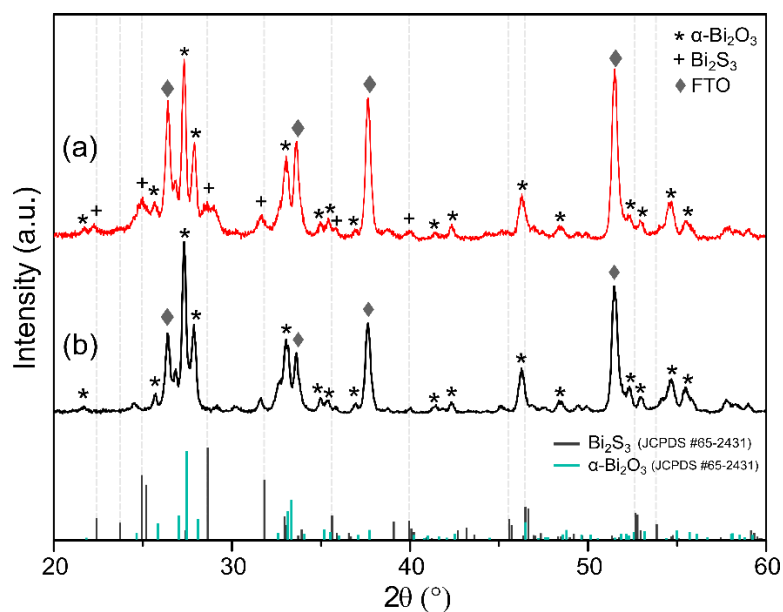


Figure S11. XRD patterns of (a) Bi-200 films oxidized at 550 $^\circ\text{C}$ for 5 h in air to produce $\alpha\text{-Bi}_2\text{O}_3$ (prior to sulfurization), and (b) after sulfurization process.

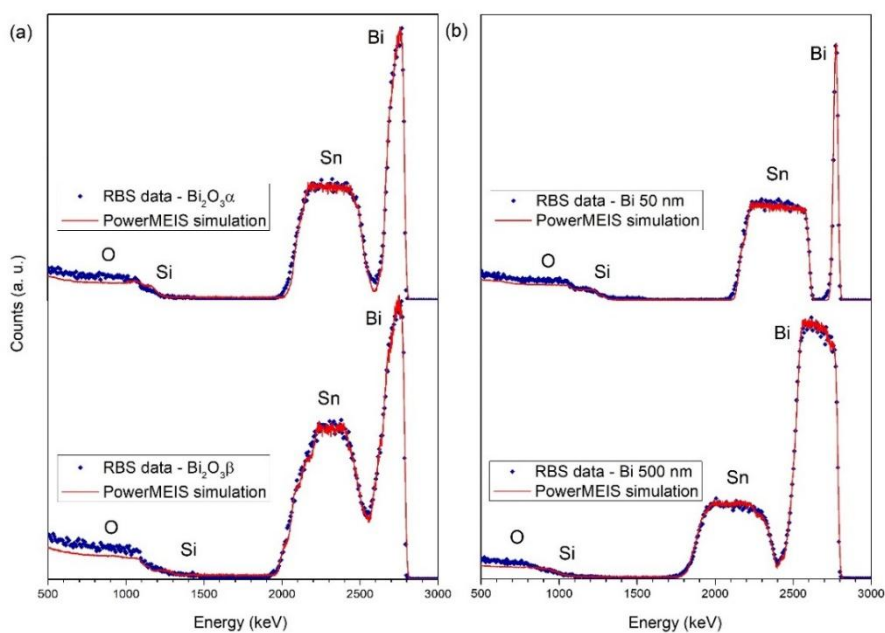


Figure S12. RBS spectra of samples Bi-50 nm and Bi-500 nm (before sulfurization) and $\alpha\text{-Bi}_2\text{O}_3\text{-}\delta\text{S}_\delta$ and $\beta\text{-Bi}_2\text{O}_3\text{-}\delta\text{S}_\delta$ (after sulfurization). Blue dots represent the raw data and the red-lines represent the corresponding simulated spectra.

Table S1. Film thickness and composition evaluated by PowerMEIS simulation of the RBS spectra presented in Figure S8.

Sample*	Elements		Thickness (nm)
	Pure film	Including diffusion	
<i>Bi</i> – 50	<i>Bi</i>	<i>Bi</i>	48
<i>Bi</i> – 200	<i>Bi</i>	<i>Bi</i>	190
<i>Bi</i> – 500	<i>Bi, O</i>	<i>Bi, O, Sn</i>	480
α – <i>Bi</i> ₂ <i>O</i> ₃ (200 nm)	<i>Bi, O</i>	<i>Bi, O, Sn</i>	200
β – <i>Bi</i> ₂ <i>O</i> ₃ (200 nm)	<i>Bi, O</i>	<i>Bi, O, Sn</i>	215
<i>s</i> – <i>Bi</i> ₂ <i>S</i> ₃ (200 nm)	<i>Bi, S</i>	<i>Bi, S, Sn, O</i>	280
α – <i>Bi</i> ₂ <i>O</i> _{3-δ} <i>S</i> _{δ} (200 nm)	<i>Bi, O, S</i>	<i>Bi, O, S, Sn</i>	230
β – <i>Bi</i> ₂ <i>O</i> _{3-δ} <i>S</i> _{δ} (200 nm)	<i>Bi, O, S</i>	<i>Bi, O, S, Sn</i>	300

*The value (200 nm) given in the first column represents the thickness of the metallic Bi film used to oxidize and/or sulfurize.

XPS measurements corroborate the sulfur distribution patterns observed through RBS analysis. The Bi 4f and S 2p spectral regions for *s*-*Bi*₂*S*₃, α -*Bi*₂*O*_{3- δ} *S* _{δ} , and β -*Bi*₂*O*_{3- δ} *S* _{δ} samples are presented in Figure S13. The *s*-*Bi*₂*S*₃ sample exhibits characteristic Bi-S bonding, with binding energies of 163.3 eV and 157.9 eV for the Bi 4f_{5/2} and 4f_{7/2} peaks, respectively, along with S 2p_{3/2} and 2p_{1/2} peaks at approximately 160.8 eV and 161.9 eV, confirming the sulfide (S²⁻) environment.² For α -*Bi*₂*O*_{3- δ} *S* _{δ} , and β -*Bi*₂*O*_{3- δ} *S* _{δ} , Bi-S peaks are shifted towards the lower binding energy, leading to the formation of sulfur-deficient species (*Bi*₂*S*_{3-x}). Additionally, the presence of Bi²⁺ species, which typically appear 0.7–1.0 eV below Bi³⁺ peaks, may also contribute to the observed spectral shifts and peak broadening. Both oxide-based samples display distinct Bi-O binding energy peaks (164.3 and 159.0 eV for 4f_{5/2} and 4f_{7/2}, respectively)

² Agata Moysowicz, ‘Scalable One-Pot Synthesis of Bismuth Sulfide Nanorods as an Electrode Active Material for Energy Storage Applications’, *Journal of Solid State Electrochemistry*, 23.4 (2019), pp. 1191–99, doi:10.1007/s10008-019-04215-7.

which are not present in the pure s-Bi₂S₃. Notably, an increase in Bi-O peak intensity of α -Bi₂O_{3- δ} S _{δ} shows a higher surface concentration of bismuth oxide compared to β -Bi₂O_{3- δ} S _{δ} .

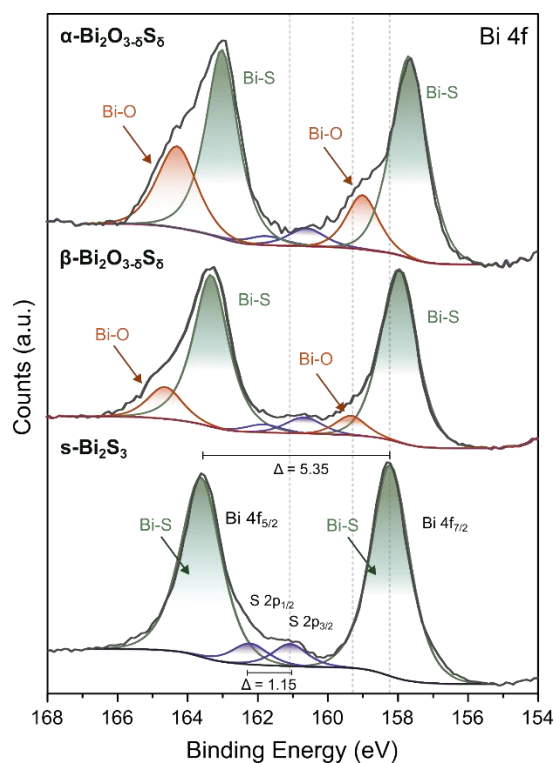


Figure S13. High-resolution XPS spectra showing the Bi 4f and S 2p regions s-Bi₂S₃, α -Bi₂O_{3- δ} S _{δ} , and β -Bi₂O_{3- δ} S _{δ} .

Open circuit potential (OCP) measurements under light On/Off were performed to evaluate the charge carrier lifetime of the samples (Figure S14a). The OCP shift upon illumination yielded values of 218 mV (s-Bi₂S₃), 95 mV (α -Bi₂O_{3- δ} S _{δ}), and 82 mV (β -Bi₂O_{3- δ} S _{δ}) vs Ag/AgCl, confirming more efficient charge separation in the metallic Bi precursor route. To obtain the time constant (τ) of the decay curve related to carrier lifetime, an exponential function was applied to fit the curves after the light was turned off (Figure S14a). The observed values of τ were found to be 21.5 s (s-Bi₂S₃), 19.8 s (α -Bi₂O_{3- δ} S _{δ}), and 8.8 s (β -Bi₂O_{3- δ} S _{δ}), indicating a significantly longer lifetime of the photogenerated charge carriers for s-Bi₂S₃. On the other hand, significantly smaller τ observed for β -Bi₂O_{3- δ} S _{δ} compared to α -

$\text{Bi}_2\text{O}_{3-\delta}\text{S}_\delta$ and $s\text{-Bi}_2\text{S}_3$ could be attributed to the intrinsic oxygen vacancies within the $\beta\text{-Bi}_2\text{O}_3$ lattice. To further demonstrate the overall stability among the precursors, a relative photocurrent loss analysis was performed, yielding 8.7% ($s\text{-Bi}_2\text{S}_3$), 10.4% ($\alpha\text{-Bi}_2\text{O}_{3-\delta}\text{S}_\delta$), and 38.4% ($\beta\text{-Bi}_2\text{O}_{3-\delta}\text{S}_\delta$), respectively (Figure S15).

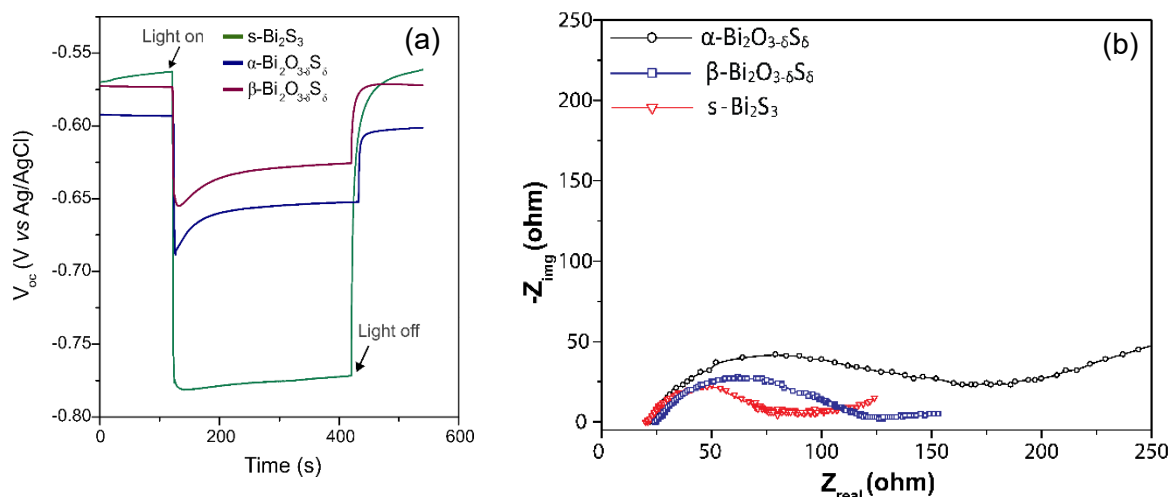


Figure S14. (a) Chronopotentiometry measurements of $s\text{-Bi}_2\text{S}_3$, $\alpha\text{-Bi}_2\text{O}_{3-\delta}\text{S}_\delta$, and $\beta\text{-Bi}_2\text{O}_{3-\delta}\text{S}_\delta$ showing open-circuit potential response to light on/off cycles. (b) Photoelectrochemical impedance spectroscopy of the films measured under 1 Sun illumination at open circuit potential from 100kHz to 100 mHz.

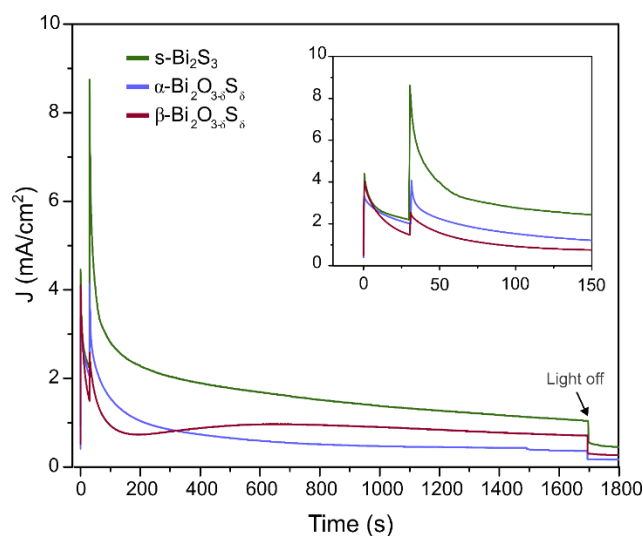


Figure S15. (b) Stability tests for direct sulfurized $s\text{-Bi}_2\text{S}_3$, $\alpha\text{-Bi}_2\text{O}_{3-\delta}\text{S}_\delta$, and $\beta\text{-Bi}_2\text{O}_{3-\delta}\text{S}_\delta$ samples (inset: amplified view of initial measurement).

Additionally, LSV measurements of $\alpha\text{-Bi}_2\text{O}_{3-\delta}\text{S}_\delta$ based on the sulfurization of $\alpha\text{-Bi}_2\text{O}_3$ oxidized at 550°C for 1 and 5 h-based are presented in Figure S16, reinforcing that improved crystallinity in the monoclinic α -phase further limits sulfur diffusion and PEC performance.

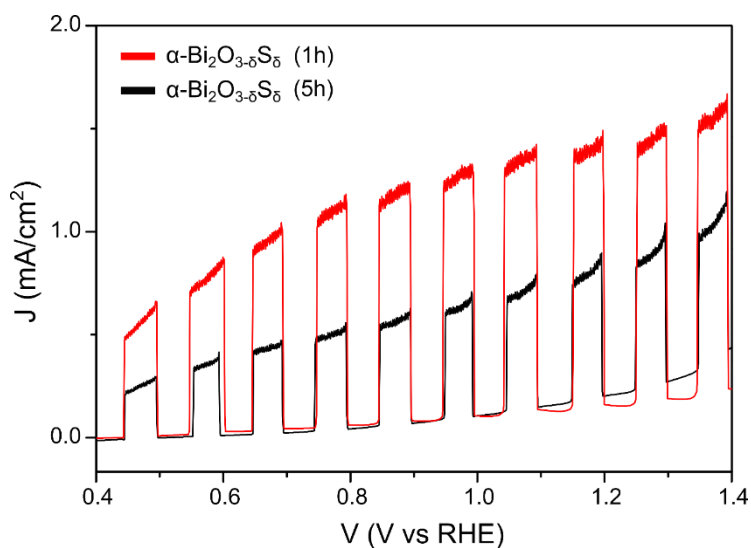


Figure S16. Chopped LSV curves of $\alpha\text{-Bi}_2\text{O}_{3-\delta}\text{S}_\delta$ samples sulfurized from $\alpha\text{-Bi}_2\text{O}_3$ prepared at 550°C for 1 h, 5 h calcination.